Prediction of uncertainty of 10-coefficient compressor maps for extreme operating conditions

Howard Cheung

Postdoctoral Research Fellow, Ray W. Herrick Laboratories, School of Mechanical Engineering, Purdue University, 177 S. Russell St., West Lafayette, IN 47907-2031, US

E-mail: cheung@purdue.edu

Christian K. Bach

Assistant Professor, Mechanical and Aerospace Engineering, Oklahoma State University, 218 Engineering North, Stillwater, OK 74078-5016

E-mail: cbach@okstate.edu

Abstract. Empirical compressor maps are a simple and reliable approach for heating and cooling system designers to estimate compressor refrigerant mass flow rate and power consumption quickly. These maps were used for a long time since most compressor manufacturers build the maps with extensive test matrices, leading to good accuracy. However, the situation changes when engineers extrapolate the maps to investigate the compressor's performance under extreme operating conditions such as for cold climate heat pump applications or under conditions with system faults. Engineers are not confident on the exact uncertainty of the extrapolation, and often claim that the inaccuracy of their studies is a result of high extrapolation uncertainty. This paper presents a method to estimate the extrapolation uncertainty due to the structure of the test matrix that trains the manufacturer maps and helps the investigators to understand if the extrapolation is the main cause of their inaccuracy. To verify that the method can estimate the uncertainty due to extrapolation, the study builds 10-coefficient compressor maps trained by different test matrices of the same size and different operating points. The maps are used to estimate the compressor performance under different operating points and their estimation uncertainties are compared. The results show that the component of the uncertainty that depends on the structure of the test matrix is small at operating conditions within the test matrix but grows significantly as the map is used to estimate outputs further away from the operating conditions within the test matrices.

1. Introduction

Empirical compressor maps for positive displacement compressors, such as the 10-coefficient polynomials outlined in ANSI/AHRI Standard 540 [1] and European Standard EN 12900 [2] are widely used in academia and industry. These maps are trained with experimental data and then used to calculate power input, mass flow rate, current, and compressor efficiency. However, the maps contain squared and cubic terms of the inputs (suction and discharge dew point temperature) and are therefore potentially inaccurate when used for extrapolation outside of the training data range. Manufacturers often state an accuracy of $\pm 5\%$ for tabulated performance data (e.g. [3] or [4]). This paper shows a method that estimates the resulting uncertainty for

the 10 coefficient polynomial at a certain point other than the training data set.
This paper does not address interpolation between different speeds of variable speed compressors. However, the shown methodology can be extended to predict the uncertainty of the outputs for interpolating between fixed speeds rather than using different fixed speed compressor maps as done by e.g. [5] and [6].

2. Linear regression

Finding the coefficients of the 10 coefficient maps can be treated as a linear regression problem, with the evaporating and condensing temperature and their linear, squared and cubed combinations being the independent variables $\vec{x}$ and the power consumption of the compressor being the estimated dependent variable y. To better understand the uncertainty sources of the model, a brief review of linear regression along with how this applies to the polynomial compressor map is shown subsequently.

2.1. Review

Linear regression is used to estimate the parameters of a linear model for a system that might have slightly nonlinear behavior. If we had the parameters $\vec{\beta}_{true}$ for the true model that is the best linear model to describe the actual system, we could use the independent inputs to our model ($\vec{x}^T$) to calculate the true output y_{true} up to an error ε caused by the difference between model and system, e.g.

$$y_{true} = \vec{x}^T \vec{\beta}_{true} + \varepsilon. \tag{1}$$

Unfortunately it is not possible to obtain the true model, since it is not possible to obtain the infinite number of input/output data points from the system. Therefore, we need to estimate the model parameters to calculate an estimate of the output. To emphasize the difference between the two models, a hat ($\hat{}$) is used for the estimated values (estimated model parameters $\hat{\vec{\beta}}$ and estimated model output $\hat{y}$), and the estimated linear model is

$$\hat{y} = \vec{x}^T \hat{\vec{\beta}}. \tag{2}$$

The parameters for the model can be estimated using measurement data. For non-weighted reduction of the squares of the errors, it can be shown that the parameter vector $\hat{\vec{\beta}}$ can be calculated as

$$\hat{\vec{\beta}} = (\mathbf{X}_{train}^T \mathbf{X}_{train})^{-1} \mathbf{X}_{train}^T \vec{y}_{train}, \tag{3}$$

where the subscript *train* is used for training data. The training data input matrix $\mathbf{X}_{train}$, composed of input data vectors $\vec{x}_{train,i}$ for each data point i is constructed as

$$\mathbf{X}_{train} = \begin{bmatrix} \vec{x}_{train,1} & \cdots & \vec{x}_{train,i} & \cdots & \vec{x}_{train,n} \end{bmatrix}^T, \tag{4}$$

where n is the total number of data points. The output training data vector is composed of output values $y_{train,i}$ for each data point as

$$\vec{y}_{train} = \begin{bmatrix} y_{train,1} & \cdots & y_{train,i} & \cdots & y_{train,n} \end{bmatrix}^T. \tag{5}$$

The accuracy of the model, measured by the mean sum of square of errors σ, is

$$\sigma = \sqrt{\frac{\Sigma_i (y_{train,i} - \vec{x}^T \hat{\vec{\beta}})^2}{n-1}}. \tag{6}$$

2.2. Polynomial compressor map as linear regression problem

ANSI/AHRI Standard 540 [1] estimates the compressor power consumption $\hat{\dot{W}}$ as

$$\hat{\dot{W}} = \hat{\beta}_1 + \hat{\beta}_2 T_{evap} + \hat{\beta}_3 T_{cond} + \hat{\beta}_4 T_{evap}^2 + \hat{\beta}_5 T_{evap} T_{cond} + \hat{\beta}_6 T_{cond}^2 + \hat{\beta}_7 T_{evap}^3 + \hat{\beta}_8 T_{evap}^2 T_{cond} + \hat{\beta}_9 T_{evap} T_{cond}^2 + \hat{\beta}_{10} T_{cond}^3, \tag{7}$$

where $\hat{\beta}_i$ are the estimated model coefficients and T_{evap}, and T_{cond} are the evaporation and condensing dew point temperatures. Referring to Eqn. (2), $\hat{\dot{W}}$ takes the place of $\hat{y}$, the estimated parameter vector $\hat{\vec{\beta}}$ is composed of the $\hat{\beta}_i$, and the vector of independent variables that contains the saturation temperature variables, $\vec{x}$, is constructed as

$$\vec{x} = \begin{bmatrix} 1 & T_{evap} & T_{cond} & T_{evap}^2 & T_{evap}T_{cond} & T_{cond}^2 & T_{evap}^3 & T_{evap}^2 T_{cond} & T_{evap}T_{cond} & T_{cond}^3 \end{bmatrix}^T. \tag{8}$$

3. Uncertainty of steady state measurements

The training data for compressor maps is obtained from steady state time series data. Steady state time series data do not show any significant monotonic trends with time but rather shows periodic and random fluctuations (noise) around an average value. The mean value a of the measured variable can be defined as

$$a = \Sigma_{i=1}^{N} \frac{a_{mea}(t_i)}{N}, \tag{9}$$

where $a_{mea}(t_i)$ is a discrete measurement of the variable at time step i, and N is the number of measurements in a time series. Measurement devices have a time-independent uncertainty often called zero-order uncertainty. The limited number of samples in combination with the fluctuations of the variable due to environmental noise leads to the first-order uncertainty. Zero-order uncertainty is typically provided by the manufacturer of the measurement device, such as $\pm 0.5K$ for T-type thermocouples, or 0.5% of the measured flow rate for Coriolis mass flow meters. First-order uncertainty is not known in advance but rather needs to be approximated by statistically analyzing the time series data of the steady state measurement. Taylor and Kuyatt (1994)[7] give the overall measurement uncertainty as

$$\Delta a = \sqrt{\Sigma_{i=1}^{N} \left(\frac{\Delta a_{mea}(t_i)}{N} \right)^2 + \left(\frac{t_{N-1,1-\alpha/2}}{N} \right)^2 \frac{\Sigma_{i=1}^{N} (a_{mea}(t_i) - a)^2}{N-1}} \tag{10}$$

where $t_{N-1,1-\alpha/2}$ is the statistic of the Student's t-distribution with a degree of freedom of N-1 and level at $1-\alpha/2$. The first part of the uncertainty is the sum of squares of the zero-order uncertainty of each observation within the steady state measurement. The second part of the uncertainty is given as the confidence interval of the average value at the level of $1-\alpha/2$. In practice, α is taken as 0.1, and a 95% confidence interval is usually used in the approximation.

4. Generating experimental results of steady state data with uncertainties from compressor map data

In this paper, no real measurement data are taken for training data, and only ideal compressor performance data from the manufacturers without uncertainty is available. In order to test the uncertainty calculation of the compressor map output, a set of training data with uncertainties is approximated from the ideal compressor performance data. If the ideal compressor performance data are the true values of the measurement, its measurement value will be different because it is

subjected to the zero-order uncertainty of the measurement device and the first-order uncertainty of the noise of the measurement environment. Assuming that the uncertainty is the confidence interval of the measurement value at a level of $1 - \alpha/2$ and the measurement value follows a normal distribution with a mean value around the true value of the measurement, the standard deviation of the normal distribution will be given by

$$\sigma_{mea} = \frac{\sqrt{(\Delta a_{zero-order}(a = a_{true}))^2 + (\Delta a_{first-order}(a = a_{true}))^2}}{z_{1-\alpha/2}} \tag{11}$$

where $z_{1-\alpha/2}$ is the z-normal distribution statistics given at a level of $1 - \alpha/2$. The observations within steady state can then be approximated by running a random number generator following a normal distribution with mean at the true value of a and standard deviation at σ_{mea} multiple times. These values can then be analyzed with the method listed in the section 3 to calculate the value and uncertainty of steady state measurement.

5. Sources of uncertainty

Uncertainty of the compressor map output is the range where the true value of the output may be relative to the map output. It consists of multiple components and can be grouped as follows:

- Uncertainty due to inputs
- Uncertainty due to training data
- Uncertainty due ot model random error
- Uncertainty due to outputs

5.1. Uncertainty due to inputs

Uncertainty due to inputs is the uncertainty propagated to the map output due to the uncertainty in the inputs to the maps. The inputs to the map (evaporating and condenser temperature) are usually obtained by converting pressure measurements to saturation temperatures with refrigerant equations of state. Therefore the estimated saturation temperature contains uncertainty from both the equation of state and the pressure measurement. The equation of state of R22 estimates saturation pressure at an uncertainty of 0.2% [7]. When the equation of state estimates an saturation temperature at a given pressure, this uncertainty is transformed into a component of the uncertainty of the saturation temperature as shown in

$$\frac{\Delta P_{sat,EOS}}{P_{sat}(T)} = 0.2\% = 0.002 \tag{12}$$

and

$$\Delta T_{sat,EOS} = \left| \frac{\partial T_{sat}(P)}{\partial P} \right| \Delta P_{sat,EOS}, \tag{13}$$

where $\Delta P_{sat,EOS}$ is the uncertainty of saturation pressure as a result of uncertainty of the equation of state, $P_{sat}(T)$ is the saturation pressure from temperature T, $\Delta T_{sat,EOS}$ is the uncertainty of saturation temperature as a result of uncertainty of the equation of state and $T_{sat}(P)$ is the saturation temperature at pressure P.

The component of the saturation temperature uncertainty due to pressure measurement is calculated by

$$\Delta T_{sat,mea} = \left| \frac{\partial T_{sat}(P)}{\partial P} \right| \Delta P_{sat,mea}, \tag{14}$$

where $\Delta T_{sat,mea}$ is the uncertainty of saturation temperature as a result of pressure measurement and $\Delta P_{sat,mea}$ is the uncertainty of pressure measurement. The overall uncertainty of the saturation temperature is given by

$$\Delta T_{sat} = \sqrt{(\Delta T_{sat,EOS})^2 + (\Delta T_{sat,mea})^2}. \tag{15}$$

The uncertainty of the map output propagated from the inputs of condensing temperature and evaporating temperature is calculated by

$$\Delta \hat{\dot{W}}_{input} = \sqrt{\left(\frac{\partial \hat{\dot{W}}}{\partial T_{evap}} \Delta T_{evap}\right)^2 + \left(\frac{\partial \hat{\dot{W}}}{\partial T_{cond}} \Delta T_{cond}\right)^2}, \tag{16}$$

where $\Delta \hat{\dot{W}}_{input}$ is the uncertainty due to inputs at the map output, ΔT_{evap} is the uncertainty of evaporating temperature at input and ΔT_{cond} is the uncertainty of condensing temperature at input.

5.2. Uncertainty due to training data

Uncertainty due to training data is the uncertainty propagated to the map output from the training data through the map coefficients. This can be understood by considering the estimation of the map coefficients as a function of the training data as

$$\hat{\vec{\beta}} = g(T_{evap,train,1}, ..., T_{evap,train,n}, T_{cond,train,1}, ..., T_{cond,train,n}, \dot{W}_{train,1}, ..., \dot{W}_{train,n}), \tag{17}$$

where n is the number of training data points. Through function g and $\hat{\vec{\beta}}$ in Eqn. (17), as suggested in [8], the uncertainty component due to training data is calculated

$$\Delta \hat{\dot{W}}_{train} = \sqrt{\begin{array}{l} \Sigma_{j=1}^{n} \left(\Sigma_{i=1}^{m} \left(\dfrac{\partial \hat{\dot{W}}}{\partial \beta_i} \dfrac{\partial \beta_i}{\partial T_{evap,train,j}} \right) \Delta T_{evap,train,j} \right)^2 \\ + \Sigma_{j=1}^{n} \left(\Sigma_{i=1}^{m} \left(\dfrac{\partial \hat{\dot{W}}}{\partial \beta_i} \dfrac{\partial \beta_i}{\partial T_{cond,train,j}} \right) \Delta T_{cond,train,j} \right)^2 \\ + \Sigma_{j=1}^{n} \left(\Sigma_{i=1}^{m} \left(\dfrac{\partial \hat{\dot{W}}}{\partial \beta_i} \dfrac{\partial \beta_i}{\partial \dot{W}_{,train,j}} \right) \Delta \dot{W}_{train,j} \right)^2 \end{array}}, \tag{18}$$

where $\Delta \hat{\dot{W}}_{train}$ is the uncertainty due to training data at the map output, $\Delta T_{evap,train,j}$ is the uncertainty of the evaporating temperature at the jth data point, $\Delta T_{cond,train,j}$ is the uncertainty of the condensing temperature at the jth data point, $\Delta \dot{W}_{train,j}$ is the uncertainty of the power consumption at the jth data point, and m is the number of coefficients in $\hat{\vec{\beta}}$.

5.3. Uncertainty due to model random error

In linear regression, the random error between true model and actual system, ε in Eqn. (1) is assumed to be normally distributed around zero with some finite variance. This variance becomes part of the uncertainty of the uncertainty of the map output and can be presented in the form of confidence intervals. Statistic textbooks [9, 10] illustrated that the confidence interval of the variance can be calculated as

$$\Delta\hat{\dot{W}}_{model} = t_{n-m,1-\alpha/2}\sigma\sqrt{1+\vec{x}^T(\mathbf{X}_{train}^T\mathbf{X}_{train})^{-1}\vec{x}} \tag{19}$$

where $\Delta\hat{\dot{W}}_{train}$ is the uncertainty due to model random error at the map output.

One significant term in Eqn. (19) is $\vec{x}^T(\mathbf{X}_{train}^T\mathbf{X}_{train})^{-1}\vec{x}$ which is the leverage of a regression model [11]. It estimates how deviated the current input vector to the map is relative to the training data of the regression model, and the magnitude of the leverage grows with the deviation. This helps to understand if the estimation is related to the training data and if (or "how much") the model is applicable at the current situation described by the input vector.

5.4. Uncertainty due to output

Uncertainty of the map output should represent the probable range where the true value lies relative to the map output. However, since the map is built from data obtained from measured power consumption instead of true values of the power consumption, the uncertainty components of the map output propagated from other sources only estimate the uncertainty of the estimation with the measured power consumption. Another component of uncertainty must be introduced so that the map output uncertainty is the uncertainty to the true map output. This uncertainty component can be approximated with the uncertainty of the measured power consumption with its true values by

$$\Delta\hat{\dot{W}}_{output} = \frac{1}{n}\Sigma_{i=1}^{n}\frac{\Delta\dot{W}_{train,i}}{\dot{W}_{train,i}}. \tag{20}$$

5.5. Overall uncertainty

The overall uncertainty of the map output is given by the square of the sum of all uncertainty components as

$$\Delta\hat{\dot{W}} = \sqrt{\left(\Delta\hat{\dot{W}}_{input}\right)^2 + \left(\Delta\hat{\dot{W}}_{train}\right)^2 + \left(\Delta\hat{\dot{W}}_{model}\right)^2 + \left(\Delta\hat{\dot{W}}_{output}\right)^2}. \tag{21}$$

6. Results and discussion

To study how this calculation method of compressor map output uncertainty helps to determine extrapolation uncertainty, the performance data of a $4.5kW$ R22 reciprocating compressor is used. The tabulated performance data shows the compressor power consumption at different evaporating and condensing temperature with a constant suction superheat 11 K within its operating range as shown in Figure 1.

Since the manufacturer data does not include experimental uncertainty, it is assumed that the data in the specification are the true values of the performance, and they are used to approximate the observations during steady state experiments with the assumptions in Table 1.

Table 1. Assumptions to approximate results in experiments of steady state compressor operation

Variable	**Zero-order uncertainty**	**First-order uncertainty**
Power consumption	0.50%	3%
Evaporating pressure	0.80%	0.9kPa
Condensing pressure	0.80%	0.4kPa

The steady state period is assumed to be 10 minutes long with data acquired at 0.1Hz in the experiment. The experimental observations at all data points in Figure 1 are generated by the method listed in Section 4.

6.1. Study cases and comparison of maps

To examine if the uncertainty of compressor map changes as the map extrapolates, various compressor maps trained from different ranges of data are compared. Six maps with different ranges of training data are designed for the study and the ranges of the training data in these maps are shown in Figure 2.

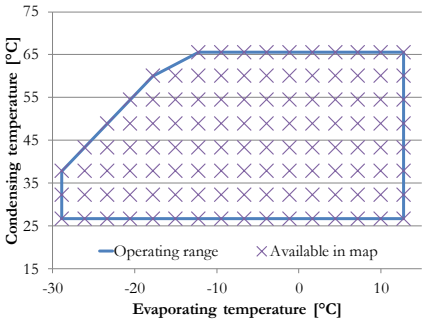

Figure 1. Operating envelope of compressor chosen for this study and available data points from manufacturer map.

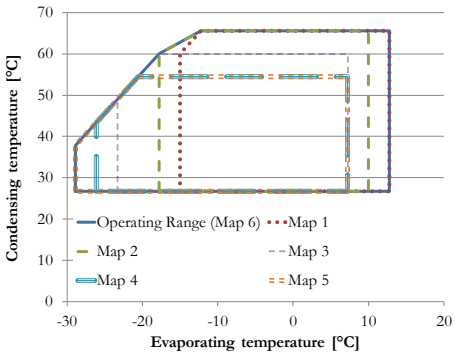

Figure 2. Range of training data for different maps.

Figure 2 shows that Maps 1 to 5 have their ranges of training data shifting from the top right-handed corner of the operating range of the compressor to its bottom left-handed corner, while Map 6 covers the entire operating range. Since it is unfair to compare maps that are generated by different number of data points, the training data points in each map are arranged such that each map contains 70 data points.

6.2. Effect of range of training data on map output

To study how the range of training data affects the extrapolation uncertainty and accuracy, the difference between the map output and approximated measurement and the map output uncertainty for all data points in Figure 1 are plotted in Figure 3, and a similar figure with their uncertainty components is plotted in Figure 4.

Figure 3 shows that inaccurate map outputs are associated with higher uncertainty and the uncertainty calculation method is a good indicator of the accuracy of the map output. Figure 4 shows that the high uncertainty of the inaccurate data points in Figure 3 are primarily a result of high uncertainty from model random error and training data.

The increase of uncertainty from model random error with inaccuracy can be explained by the leverage term $\vec{x}^T(\mathbf{X}_{train}^T\mathbf{X}_{train})^{-1}\vec{x}$ in Eqn. (19) which increases as the map extrapolates, and map extrapolation results in lower accuracy. Hence the uncertainty from model random error increase with a decrease of the map accuracy and applicability.

To explain the increase of uncertainty from training data with a decrease of map accuracy in Figure 4, the squared terms in Eqn. (18) are labeled as uncertainty from training data per measurement, and their values from two map outputs of Map 1 are plotted as Figures 5 and 6.

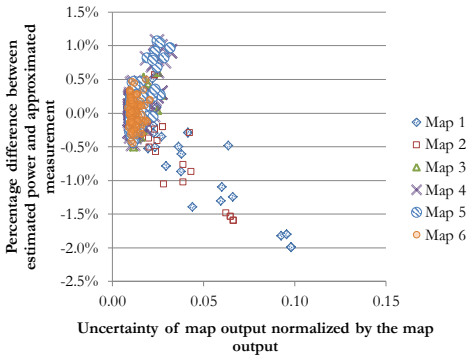

Figure 3. Change of accuracy of maps with output uncertainty in different maps.

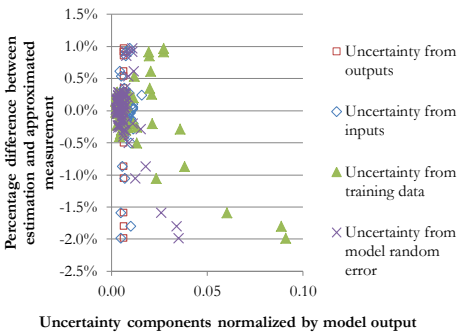

Figure 4. Change of accuracy of maps with different uncertainty components.

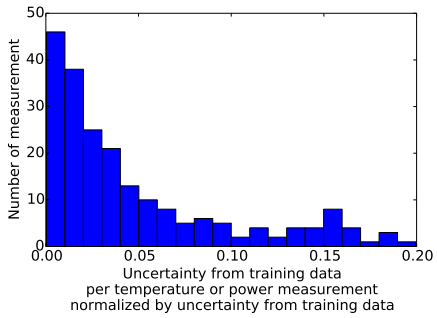

Figure 5. Histogram of uncertainty terms in Eqn. (18) for $T_{evap} = -1.1°C$ and $T_{cond} = 60.0°C$.

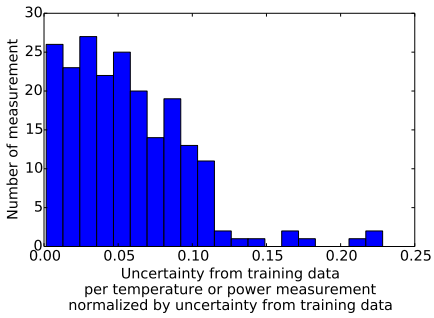

Figure 6. Histogram of uncertainty terms in Eqn. (18) for $T_{evap} = -28.9°C$ and $T_{cond} = 26.7°C$.

Figure 5 shows a histogram that is more left-skewed than Figure 6. This is because Figure 5 is obtained from a data point inside the training data range of Map 1 (see Figure 2), and the map only needs information from a few data points around $T_{evap} = -1.1°C$ and $T_{cond} = 60.0°C$ to estimate its map output. Hence the estimation does not depend on most of the data points, and their training data uncertainties do not propagate to the map output as shown by Figure 5.

However, Map 1 extrapolates to the lower left handed corner in Figure 2 for the condition in Figure 6, and the estimation is significantly affected by multiple data points in the training data. If any of these significant training data points change, the estimation result at this condition will be changed significantly. Hence much more training data points propagate their uncertainty to the map output under the condition in Figure 6 than that in Figure 5. This also explains that the uncertainty of training data is a significant component in the extrapolation uncertainty of the map output, and the uncertainty increases as the map applicability and accuracy decrease.

6.3. Effect of number of training data points on map output

To understand how the number of training data points affect the map output, another map (Map 7) was created with the same range of training data as Map 1 and 24 data points only, as shown in Figure 7. The accuracy of Map 7, rated by coefficient of variation *cov* as

$$cov = \frac{\text{Mean of the sum of squares of errors}}{\text{Mean value of estimated values}} = \frac{\sigma}{1/n \cdot \Sigma_1^n \hat{y}_i} \tag{22}$$

is compared with that of Map 1 in Table 2.

Table 2. Accuracy of Maps 1 and 7.

Map	Coefficient of variation based on training data poinst only (cov_{train})	Coefficient of variation based on all data points in Figure 1 (cov_{all})
Map 1	0.18%	0.31%
Map 7	0.17%	1.10%

Table 2 shows that the accuracy of Map 7 is similar to that of Map 1 at the training data points, but the analysis with all available data points shows that Map 7 is less accurate than Map 1. This shows that using fewer training data points reduces map accuracy. To understand if it is related to extrapolation, the difference between the power consumption estimation and their approximated measurement with the distance, e.g. $\sqrt{\Delta T_{cond}^2 + \Delta T_{evap}^2}$, from the nearest training data point as shown in Figures 8 and 7.

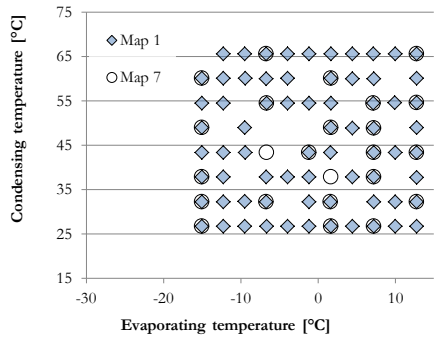

Figure 7. Training data points for Maps 1 and 7. Note the absence of low temperature training data.

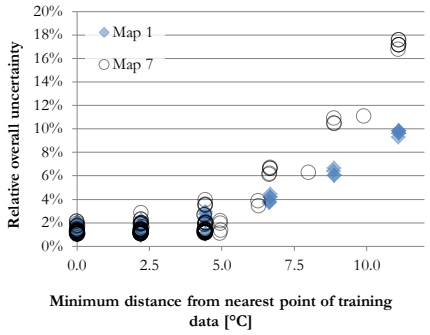

Figure 8. Change of accuracy with distance to nearest training data point for maps 1 and 7.

As shown in Figures 8 and 7, although the range of training data points in both maps is the same, the effect of the reduced number of points in the training data is pronounced for large distances (e.g. extrapolated outside training data range of map) of 10°C or larger and can increase the uncertainty from 10% (Map 1) to around 17% (Map 7) in the most extreme case.

This shows that the inaccuracy due to the reduction of training data can be shown by uncertainty. To understand why uncertainty can show this, Figures 9 and 10 are plotted.

Figures 9 and 10 show that both the accuracy of Maps 1 and 7 decreases as their uncertainty from model random error and the uncertainty from training data increase, and the reduction of Map 1 accuracy in both figures are more rapid than Map 7. This shows that Map 7, despite having the same training data range as Map 1, is less applicable and accurate as Map 1. This shows that extrapolation uncertainty and accuracy are not only affected by the range of training data but also the number of training data points.

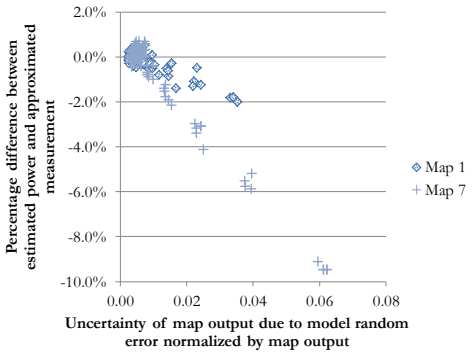

Figure 9. Change of accuracy of maps with uncertainty from model random error in Maps 1 and 7.

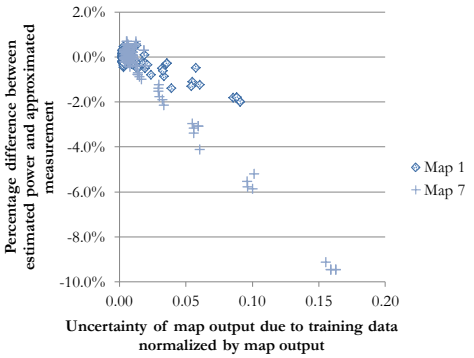

Figure 10. Change of accuracy of maps with uncertainty from training data in Maps 1 and 7.

7. Conclusions

To conclude, this paper demonstrates how uncertainty of 10-coefficient compressor maps can be calculated based on the uncertainty due to inputs, the uncertainty due to model random error, the uncertainty due to training data and the uncertainty from outputs. It shows a method to assess the acuracy and applicability of the map output under extrapolation without measuring the output variable. It also shows that the range of training data and the number of training data points affect the accuracy and applicability of the map.

8. Future work

One of the basic assumptions in this paper is that individual measurement values are normally distributed around their average value. However, this might not be the case for actual measurement data. Therefore, experiments with actual compressor measurements should be conducted to check whether this assumption is appropriate.

References

[1] ANSI/AHRI standard 540: 2004 standard for performance rating of positive displacement refrigerant compressors and compressor units.

[2] EN 12900:2013. Refrigerant compressors - rating conditions, tolerances and presentation of manufacturer's performance data.

[3] Emerson Climate Technologies 2006 Copeland CF and CS compressors 50 hertz - the final solution for HFC performance. Tech. rep. Sidney, Ohio

[4] Bristol Compressors International Inc 2015 Performance table for H23A463DBL, revision 5. Tech. rep.

[5] B Shen, O Abdelaziz, and C K Rice 2014 Compressor selection and equipment sizing for cold climate heat pumps. *2014 IEA HP conference*

[6] S L Caskey, D Kultgen, E A Groll, W Hutzel, and T Menzi 2012 Simulation of an air-source heat pump with two-stage compression and economizing for cold climates.

[7] B N Taylor and C E Kuyatt 1994 *NIST Technical Note 1297, 1994 Edition: Guidelines for Evaluating and Expressing the Uncertainty of NIST Measurement Results* (Gaithersburg: National Institute of Standards and Technology)

[8] L Song, G Wang, and M R Brambley 2013 *HVAC&R Research* **19** 335 – 345

[9] D C Montgomery 2005 *Design and Analysis of Experiments.* 6th ed (Jon Wiley & Sons)

[10] F A Graybill and H K Iyer 1994 *Regression Analysis: Concepts and Applications.* (Duxbury Pr)

[11] A C Atkinson 1987 *Transformation and Regression.* (Oxford Statistical Science Series)